

A Triboelectric–Electromagnetic Hybrid Nanogenerator with Broadband Working Range for Wind Energy Harvesting and a Self-Powered Wind Speed Sensor

Cuiying Ye,^δ Kai Dong,^δ Jie An,^δ Jia Yi, Xiao Peng, Chuan Ning, and Zhong Lin Wang*



Cite This: *ACS Energy Lett.* 2021, 6, 1443–1452



Read Online

ACCESS |



Metrics & More

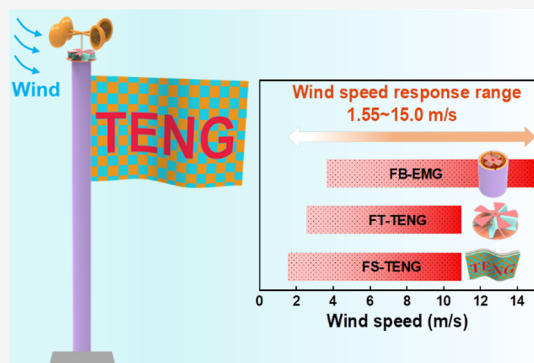


Article Recommendations



Supporting Information

ABSTRACT: Wind energy plays an increasingly important role in alleviating the shortage of fossil fuel energy because of the emerging promising technologies such as electromagnetic generators (EMGs), triboelectric nanogenerators (TENGs), and their hybrid nanogenerators, but only part of wind energy can be effectively converted into electricity. Here, a triboelectric–electromagnetic hybrid nanogenerator (FTEHG) is reported with wide working range of wind speed for effectively harvesting various levels of wind energy, such as breezes and moderate and strong wind. It is verified that the FTEHG can effectively integrate the superiority of EMG at high frequency and TENG at low frequency, enhancing the entire energy output performance and broadening the working range of wind speed from 1.55 to 15 m s⁻¹. The FTEHG has been demonstrated to successfully and continuously power a digital thermometer and was used as a self-powered wind speed sensor, which has application prospect in comprehensive weather monitoring with a self-powered and real-time manner.



With the rapid development of modern society, the world is gradually entering the era of big data, internet of things, and artificial intelligence, in which the demand for energy that is clean, renewable, continuous, and distributed takes on greater significance and urgency for powering distributed sensor networks. The conventional method for powering hundreds of millions of sensors is applying batteries, which have limited lifetime and need constant monitoring and replacement, resulting in a tremendous maintenance cost and possibly causing environmental pollution. This is not the most ideal solution to solve the energy supply issues for distributed sensors. Harvesting energy from ambient environment of the electric devices, such as wind, solar, mechanical vibration, water flow energy, and so on, is an alternative strategy.¹ As one of the clean, renewable, and widespread natural resources in environment, wind energy shows great potential to solve these problems.² In particular, for the hundreds of millions of sensors, the energy requirement of each individual unit is low, making it possible to supply the required energy by harvesting the wind energy around these sensors. In 2012, triboelectric nanogenerators (TENGs, also called Wang generators) have been invented for effectively converting ambient mechanical energy into electricity based on

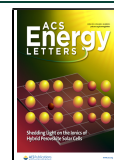
the coupling effect of triboelectrification and electrostatic induction.^{3,4} With the merits of low cost and weight and high conversion efficiency, especially at low frequency, the TENG has been demonstrated as a sustainable energy-harvesting technology for capturing the surrounding mechanical energy, such as human motion,^{5–7} mechanical vibration,⁸ ocean waves,⁹ and light breezes.^{10,11}

In this context, many structures have been exploited to effectively harvest wind energy based on TENGs.^{12,13} Yang et al. designed a TENG with a structure of fluorinated ethylene propylene film between two aluminum foils, which can effectively improve the film vibration frequency.¹⁴ Wang et al. provided a rotary structure TENG, which can harvest any orientation wind energy, where a soft friction mode instead of traditional rigid friction mode was used to decrease the friction

Received: February 3, 2021

Accepted: March 16, 2021

Published: March 25, 2021



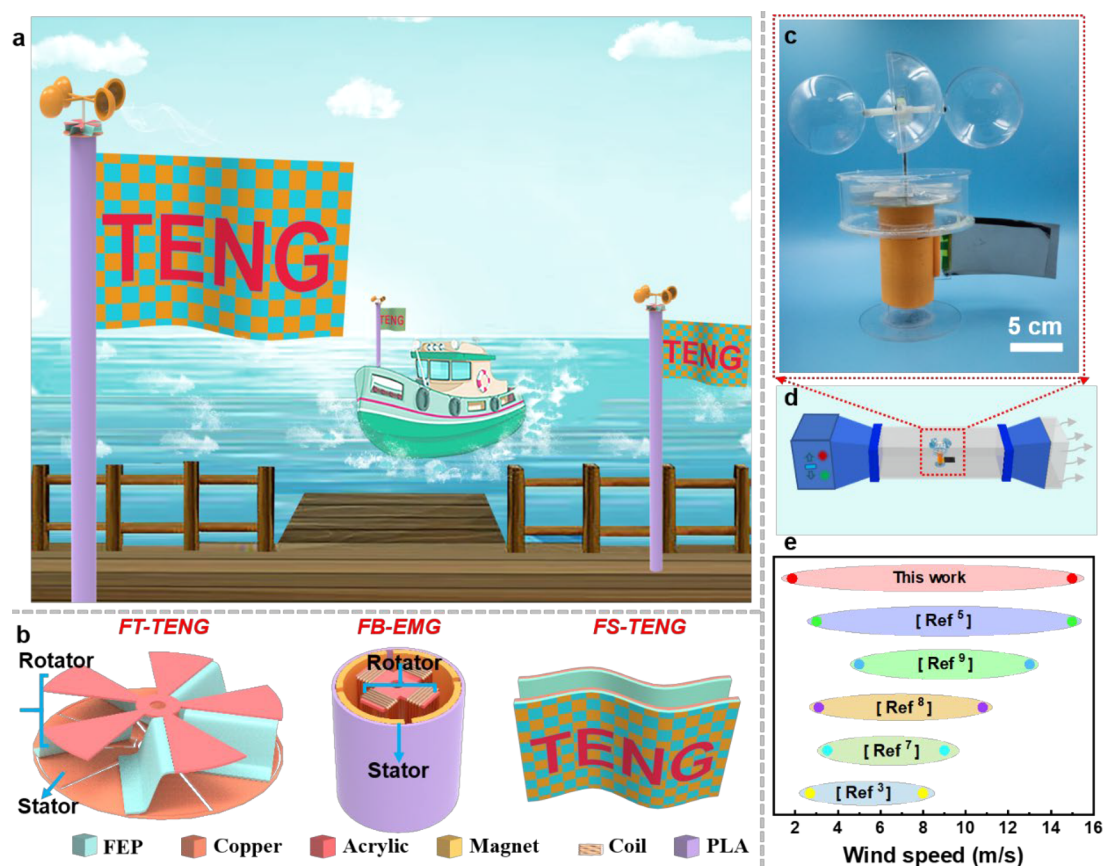


Figure 1. Architectural characteristics of the FTEHG for broadband wind energy harvesting. (a) Application scenario of the FTEHG on a ship and in a port. (b) Detailed structural information on the three parts: FT-TENG, FB-EMG, and FS-TENG. (c) Photograph of the FTEHG (scale bar, 5 cm). (d) Wind tunnel for measuring the electrical output performance of FTEHG. (e) Comparison of the working wind speed ranges between the representative works and our work to verify the characteristics of the broadband working range.

resistance.¹⁵ Sun et al. provided a fully flexible fluttering-double-flag type TENG based on contact–separation mode for low wind speed energy harvesting.¹⁶ Although intensive efforts have been devoted to improving the performance of TENG for wind energy harvesting, it still has limited output performance so that it cannot be utilized to sustainably power those electronics with large energy demand in a reliable and self-powered manner.

Hybridizing a TENG with other energy-harvesting technologies, such as piezoelectric nanogenerators (PENGs),^{17–24} solar cells,²⁵ and electromagnetic generators (EMGs),^{26–28} is a better strategy to alleviate this troublesome issue in the short term. Among them, the combination of EMGs and TENGs can provide preferable energy conversion efficiency and complement their respective advantages.^{29–31} A theoretical comparison between TENGs and EMGs was reported by Zhang et al., which indicated a comparative and symmetric relationship between EMG and TENG.³² Zi et al. systematically compared the performance of EMGs and TENGs under low-frequency motion (<5 Hz) by theoretical model and experiments, demonstrating the superior characteristics of TENGs in low frequency and EMGs in high frequency.³³ Some progress has been achieved also based on the hybridization of TENGs and EMGs for wind energy harvesting. Wang et al. reported an ultralow-friction hybrid nanogenerator by introducing the soft and elastic contact between two friction materials to improve its output performance.³⁴ Zhang et al. provided a windmill-like hybrid nanogenerator to successfully prevent rotation resist-

ance induced by the friction between rotor and stator in the conventional structures.³⁵ Fan et al. has constructed a packaged hybrid nanogenerator consisting of two TENGs and two EMGs for better output performance and isolation from the harsh environment.³⁶ Although a high output performance can be obtained in a relative narrow wind speed range, a part of wind energy cannot be harvested. In addition, the multistage hybrid nanogenerators, which can not only improve the whole energy conversion efficiency but also broaden the device working frequency range, have rarely been reported, especially for gentle wind less than 3 m s^{-1} , which is approximately the annual mean surface wind speed in most regions on the earth.³⁷ More importantly, hybridized energy-harvesting technologies can improve the reliability of dealing with unstable energy inputs, realizing a sustainable, reliable, and self-powered energy supply, which is very significant for sensor networks.

Here, a triboelectric–electromagnetic hybrid nanogenerator (FTEHG) is designed for broadband wind energy harvesting and self-powered wind speed sensing. Owing to the characteristics of high efficiency of TENG at low frequency and the high performance of EMG at high frequency, the FTEHG can not only efficiently harvest high wind speed energy (usually more than 5 m s^{-1}) but also scavenge low wind speed energy, which is approximately the annual mean wind speed in most regions. In particular, the wind speed response range is extended to a wider range from 1.55 m s^{-1} to 15 m s^{-1} , allowing breezes and moderate and strong wind to be efficiently harvested. The

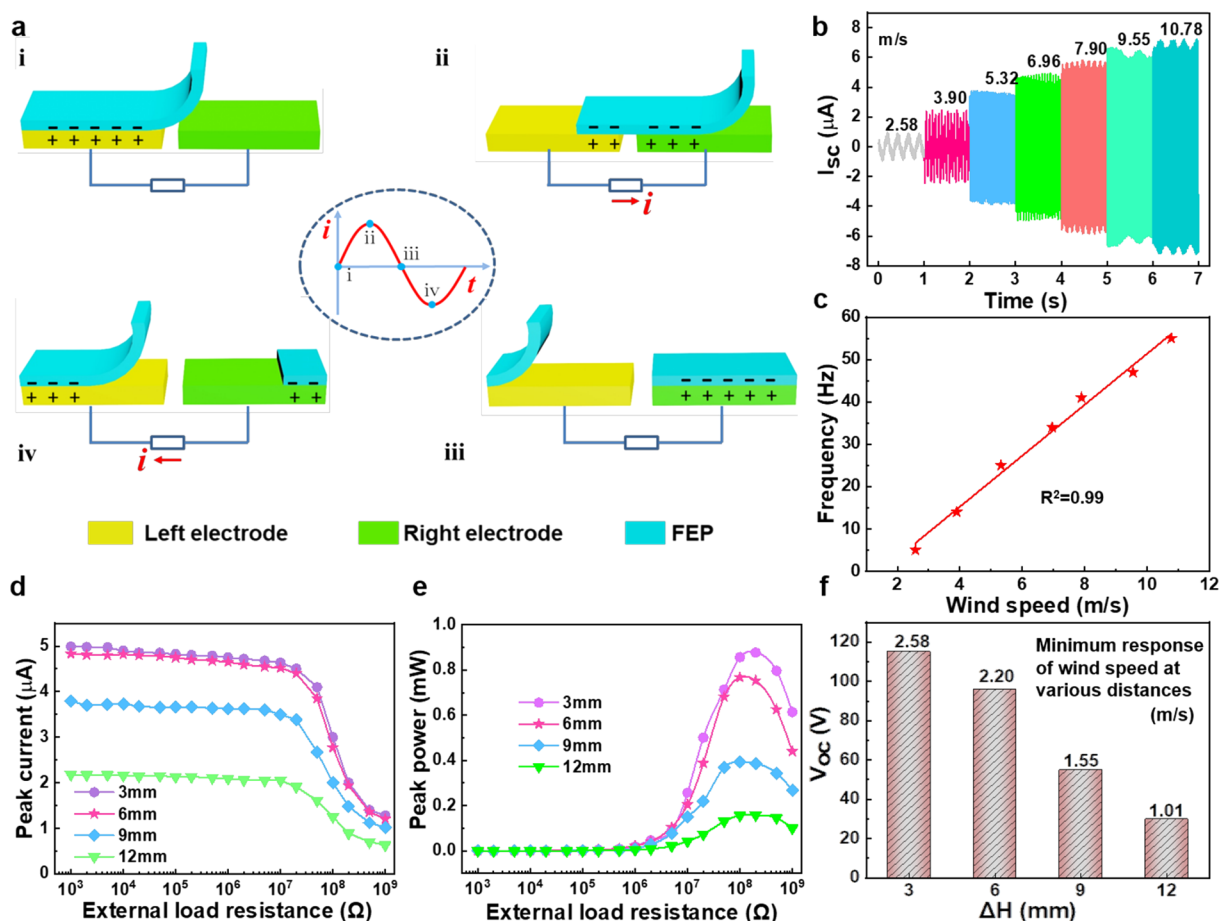


Figure 2. Working mechanism and electrical output performance of the FT-TENG. (a) Working mechanism of the FT-TENG under rotation condition. (b) Short-circuit current of the FT-TENG at various wind speeds. (c) Real corresponding frequency of FT-TENG at various wind speeds. (d) Output current and (e) output power of FT-TENG with different distances between the rotator and stator at various load resistances. (f) Open-circuit voltage of the FT-TENG with various distances between the rotator and stator at the minimum response of wind speed.

FTEHG is composed of three parts, i.e., flag top triboelectric nanogenerator (FT-TENG), flag body electromagnetic generators (FB-EMG), and flag surface triboelectric nanogenerator (FS-TENG). The all-in-one power source can generate an average output power of 0.23, 0.52, and 0.07 mW at the wind speed of 6.96 $m s^{-1}$, respectively, which can be used in a single manner or hybridized with power management to continuously power a thermometer. In addition, because of the linear relationship between the movement frequency and wind speed, the FTENG has been demonstrated as a successful real-time wind speed sensor. This work provides an effective way for wide working scope wind energy harvesting, which has application potential in fully automated and comprehensive weather monitoring in the future.

Structural Diagram of the FTEHG. Combining the advantages of TENGs at low frequency and EMGs at high frequency, the FTEHG has been demonstrated as a power source to drive electronic devices, especially in remote areas. To achieve the high efficiency, sustainability, and broadband of the power source, a hybridized nanogenerator is elaborately designed. A schematic illustration and typical application scenarios are shown in Figure 1a. The all-in-one structure can be located in ports upon easy integration with a light pole and also installed on ships for offshore wind energy harvesting.

As depicted in Figure 1b, the hybrid nanogenerator is mainly composed of three parts: FT-TENG, FB-EMG, and FS-TENG. The rotary mode has been widely used for wind energy harvesting, such as the electromagnetic wind turbine. Considering the structural stability, high frequency, and high efficiency of the rotary mode, the rotary mode TENG and EMG are first introduced as the main structure. Given the effect of frictional resistance on starting wind speed of energy harvester, in contrast to the conventional disk–disk rotary mode TENG, a rotary mode TENG with suspended polymer film as the triboelectric layer was chosen to reduce the operating frictional resistance, decrease the starting wind speed to enhance the energy output, and increase service life. As shown in Figures 1b and S1a, the FT-TENG is constituted by a rotator and a stator. The stator is fabricated by a commercialized printed circuit board (PCB) with 10 radially arrayed copper sectors as the contact electrode. Five pieces of FEP thin films as the contact dielectric layer are fixed on the rotator. In addition, a rotary EMG as the complementary energy harvester of TENG is suitable for effective harvesting of wind energy, especially in the strong wind environment. The introduction of EMG enables the system to power electronics with a greater power demand. Similarly, the FB-EMG part also consists of a rotator and a stator (Figures 1b and S1b). The rotator is composed of a shaft and a cross-shaped structure

with four symmetrical distributed homemade coils, which are connected in series to increase the FB-EMG's final output voltage. Four pieces of arc-shaped magnets are attached on the inner wall of the stator, which is made by 3D printing with a polylactic acid (PLA) material. Particularly, the poles of two adjacent magnets are opposite. The rotators of the FB-EMG and FT-TENG have the same shaft, as shown in Figure 1a. Once the wind cup is driven by the wind, the rotators of the FT-TENG and FB-EMG will follow the wind cup to revolve.

Because the rotary mode TENG has a starting wind speed, and it may be further enhanced because of the introduction of EMG, the system might not operate at low wind speed, especially for breeze wind energy harvesting. Usually, thin polymer film has light and soft feature which can easily flutter in air flow. With the merits of low starting wind speed and high efficiency at low frequency, introducing a swing mode TENG can help address the problem of energy slump and improve the reliability of the whole system, realizing fully self-powered systems. The fabricated double-flag type TENG is constituted of two FEP films with Cu as the back electrode to harvest breeze energy (Figures 1b and S1c). The surface topography of the FEP film is characterized and shown in Figure S1c, indicating that microstructure existed on its surface, which contributes to the superior electric output performance of the two TENGs.

Figure 1c shows a photograph of the real device, and a wind tunnel is used for testing the electrical output performance (Figure 1d). To verify the characteristics of the FTEHG with broadband response to wind speed to harvest high- and low-frequency wind energy, the working scope of the device was compared with previous representative works, indicating that our FTEHG has superior performance for wide speed range wind energy harvesting. The detailed description is illustrated in Figure 1e and Table S1. In addition, the comparison of the output performance and the advantages and disadvantages between the FTEHG with previous representative hybrid generators is provided in Table S2. Similar to solar cells used to harvest different wavelengths of sunlight to enhance the energy conversion efficiency as much as possible, the broadband working scope of FTEHG from 1.55 to 15 m s⁻¹ can effectively harvest wind energy and increase the final energy output, showing great potential in collecting various levels of wind energy for practical applications.

Working Mechanism and Electrical Output Performance of the FT-TENG. To maximize the energy capture efficiency, two TENGs with different modes and one EMG are integrated into this hybrid nanogenerator. In comparison with the contact-separation mode TENG, the rotary mode TENG has higher electrical output, which is very convenient for environmental energy harvesting, such as wind and water flow. Here, a FT-TENG with low friction resistance is placed on the top of our hybrid nanogenerator for harvesting energy and remote sensing. As shown in Figure 2a, the electricity generation process is illustrated under the relative rotary motion between the FEP films and Cu electrodes. At the initial state, the FEP film is fully overlapped with the left electrode, where negative triboelectric charges are generated on the surface of the FEP film and an equal number of positive charges are produced in the left electrode because of the triboelectrification effect. As the FEP film slides toward the right electrode, the generated positive charges on the left electrode will flow to the right electrode in an external circuit to balance the electric potential between the two electrodes.

When the FEP film is completely overlapping with the right electrode, all of the positive charges in the left electrode will be driven to the right electrode, which is regarded as the half cycle of electricity generation. Then, as the rotator continues to rotate, the FEP film will cross the right electrode to the next left electrode, generating a reverse output current in the external circuit. This is the whole working process for electricity generation. Figure S2 presents the finite element analysis method by COMSOL software to simulate the potential distributions between the FEP film and Cu electrodes during the rotation process to verify the working mechanism of the FT-TENG.

The output performance of the FT-TENG was measured in a wind tunnel. To avoid the FEP film from being floated without contacting with the electrode at wind directly, the FT-TENG was further wrapped by an acrylic hood, as shown in Figure S7. The wind speed and the vertical distance between the rotator and stator of FT-TENG are optimized to improve the output performance of FT-TENG. Figure 2b shows the short-circuit current (I_{sc}) of the FT-TENG at various wind speeds, from 0.9 μ A at 2.58 m s⁻¹ to 7.2 μ A at 10.78 m s⁻¹. The corresponding open-circuit voltage (V_{oc}) and short-circuit transferred charges (Q_{sc}) remain nearly constant at different wind speeds because they are determined by the surface charge density. In contrast, the I_{sc} is not only dependent on the charge density but also related to the charge-transfer rate. The matched resistance and corresponding peak output power are 100 M Ω and 0.88 mW at the wind speed of 6.96 m s⁻¹, respectively (Figure S4). In addition, we observed that the revolving frequency of the FT-TENG increases linearly with the wind speed (Figure 2c), which indicates that it can be used as a wind speed sensor unit. Furthermore, the vertical distance between the rotator and stator has an obvious effect on the real contact area, which is an extremely important parameter to optimize the output performance of the FT-TENG. The output performance of FT-TENG at various distances between the rotator and stator (3, 6, 9, and 12 mm) are measured at the same conditions (Figure S3), which shows that the V_{oc} , I_{sc} , and Q_{sc} decrease from 124 V, 5 μ A, and 45 nC at 3 mm to 34 V, 2 μ A, and 14 nC at 12 mm under a constant wind speed of 6.96 m s⁻¹, and the output power (Figure 2d,e) also decreases with the increasing of the distance. In this work, we choose 3 mm as the appropriate parameter for obtaining a high electric output. In addition, we find that the minimum responsive wind speed of FT-TENG also decreases with the increase of the distance between rotator and stator (Figures 2f and S5), which means that we can adjust the distance to decrease the minimum responsive wind speed, by which the FT-TENG can harvest lower wind speed energy. In addition, the durability of the FT-TENG is tested at 6.96 m s⁻¹ for 60 min (about 140 000 cycles), and the output performance of the FT-TENG remains stable (Figure S6), showing great potential for practical application.

Working Mechanism and Electrical Output Performance of the FB-EMG. EMG has high energy conversion efficiency at high wind speed. Its V_{oc} and I_{sc} of each coil are defined as

$$V_{oc}^{EMG} = -N \frac{d\Phi_B}{dt} \quad (1)$$

$$I_{sc}^{EMG} = \frac{V_{oc}^{EMG}}{R} \quad (2)$$

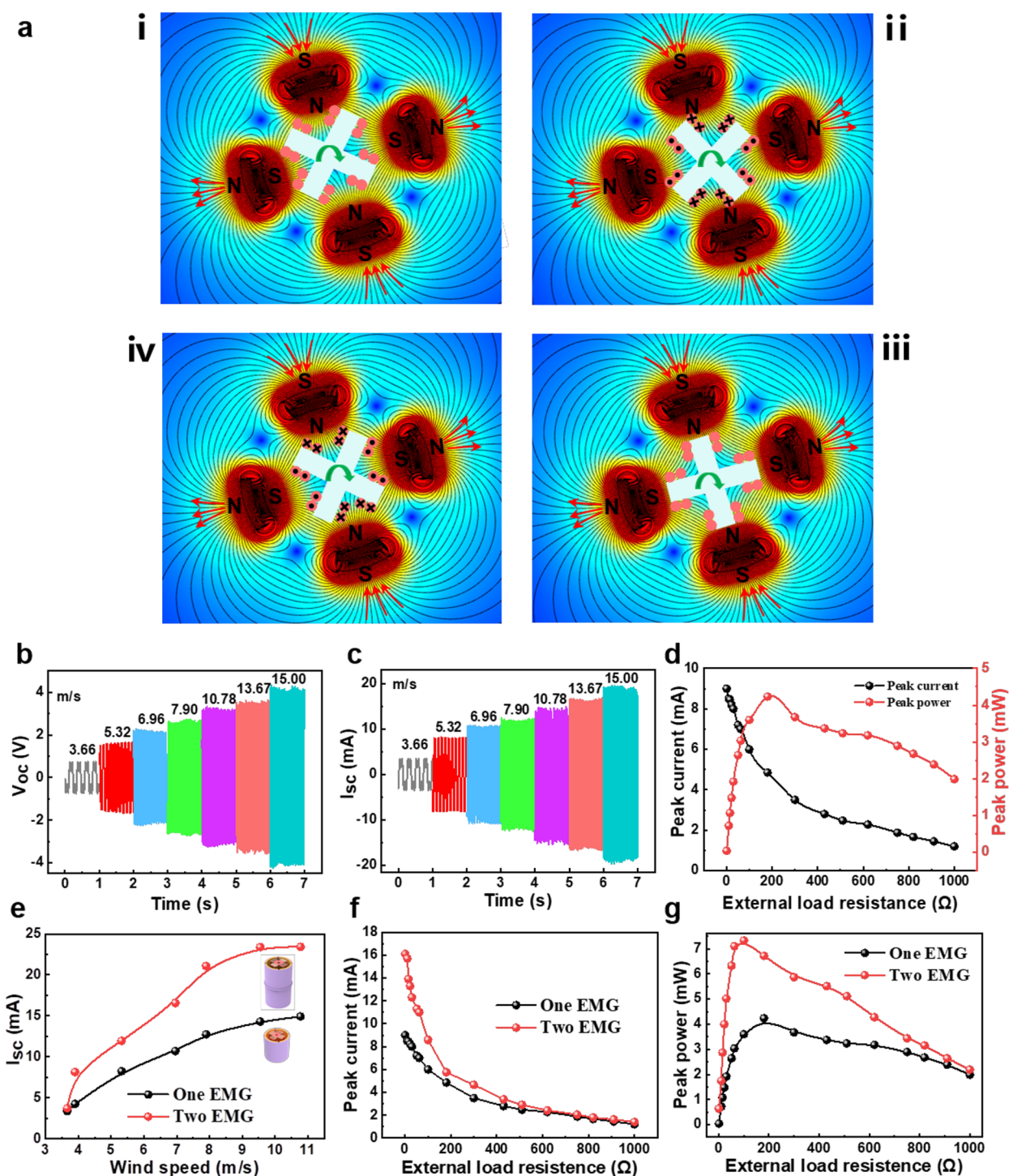


Figure 3. Working mechanism and electrical output performance of the FB-EMG. (a) Schematic diagram of simulated magnetic flux distribution and working principle of the FB-EMG. (b) Open-circuit voltage and (c) short-circuit current of the FB-EMG at various wind speeds. (d) Output current and power of the FB-EMG with various load resistances. (e) Open-circuit voltage of one and two FB-EMGs at various wind speeds. (f) Output current and (g) power of one and two FB-EMGs with different load resistances.

where Φ_B is the total magnetic flux in each coil, N the number of each coil, and R the internal resistance of coils. The working mechanism of FB-EMG is illustrated in Figure 3a. In the initial state, the coil is in the middle of the adjacent magnets as shown in Figure 3a(i). When the coil starts to rotate, the coil generates induced current because of the change of the magnetic flux passing through the coil. As indicated in Figure 3a(ii), the direction of the induced current in the adjacent coil

is opposite because the adjacent magnets have opposite magnetic polarity. Subsequently, the magnetic flux passing through the coil continues to increase until the coil locates in the middle of one magnet which is the threshold between magnetic flux increase and decrease, and the induced current reaches zero (Figure 3a(iii)). As the coil spins toward the next magnet, the magnetic flux passing through the coil continues to decrease, and an opposite current is generated (Figure 3a(iv))

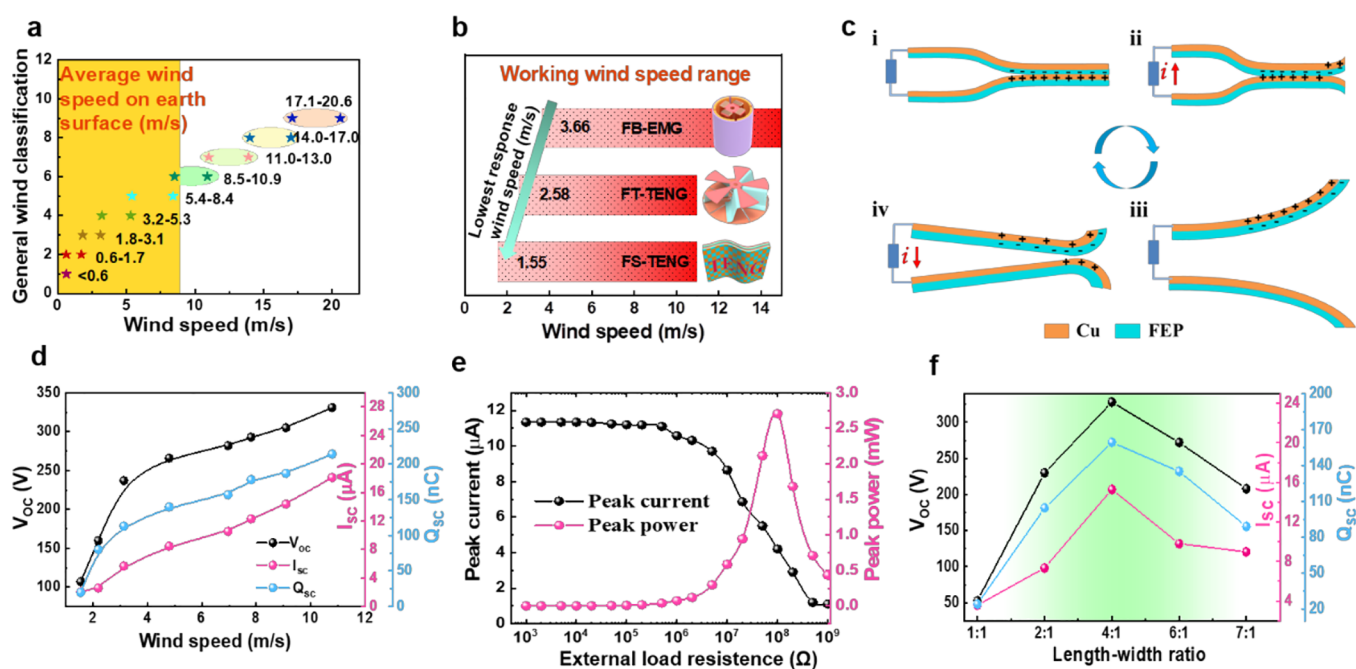


Figure 4. Output characteristics of the FS-TENG. (a) Wind classification and corresponding wind speed range. The luminous yellow area is the average wind speed on earth in which wind energy can be effectively harvested by TENG, and the part of the energy over the wind speed can be effectively scavenged by EMG. (b) Working range of wind speed of the three generators, which indicates that the FS-TENG has the minimum response wind speed. (c) Working mechanism of the FS-TENG. (d) Open-circuit voltage, short-circuit current, and short-circuit transferred charges of the FS-TENG at various wind speeds. (e) Output current and power of the FS-TENG with different load resistances. (f) Optimization of the output performance of FS-TENG by the length–width ratio.

until the coil arrives in the next middle of adjacent magnets. This is the whole working mechanism of the FB-EMG. From Figure 3b,c, we noticed that the V_{oc} and I_{sc} increase with wind speed from 0.74 V and 3.54 mA at 3.66 m s^{-1} to 4.3 V and 19.5 mA at 15 m s^{-1} . The peak current and power of the FB-EMG is 4.85 mA and 4.23 mW with the external resistance of 100Ω under the wind speed of 6.96 m s^{-1} .

In addition, two FB-EMGs were integrated into one flagpole to increase the total output performance of the FB-EMG. It can be found that the I_{sc} and power density of the FB-EMGs with two integrated units are greater than those of the EMG with one unit (Figures 3e–g, S8, and S9), which indicates that the output performance of the FB-EMG can be rapidly enhanced in parallel and the lowest working frequency is rarely changed. Because the frequency of the FB-EMG also keeps a linear relationship with the wind speed, the FB-EMG also can be used as a wind speed sensor.

Working Mechanism and Electrical Output Performance of the FS-TENG. Generally, the wind speed for operation of an EMG should be greater than $3.5\text{--}4.0 \text{ m s}^{-1}$, which is greater than the normal wind speed in most regions.³⁷ For example, the annual average wind speed of Beijing is about 2.0 m s^{-1} and decreases at a rate of 0.1 m s^{-1} every ten years.³⁸ Therefore, it is difficult for EMGs to effectively harvest this kind of wind energy. Figure 4a and Table S3 present a summary of the classification of wind and corresponding flow speed as well as visible natural phenomenon on the earth. Obviously, the normal wind on land and ocean surface is a breeze (about 5 m s^{-1}), which is also less than the optimal working wind speed range of EMG, while TENG can effectively operate in this wind range. To harvest breeze energy for practical applications, the FS-TENG is designed. From the wind speed response of FT-TENG, FB-EMG, and

FS-TENG (Figure 4b), the FS-TENG has the minimum lowest response wind speed of 1.55 m s^{-1} , which is lower than that of most previous works.

Figure 4c describes the working mechanism of the FS-TENG, which includes four working states in one period. When the FEP film contacts with the Cu electrode, the same amount of negative and positive charges is generated on the surface of the dielectric layer and Cu electrode because of the triboelectrification effect, as shown in Figure 4c(i). Once the input wind energy drives the FEP films to vibrate and then separate from each other, the electrons on the upper electrode will flow to the lower electrode via the external load, generating forward current, as shown in Figure 4c(ii). When two FEP films are completely separate, electrostatic balance will be achieved, and there will be no current in the external circuit, as shown in Figure 4c(iii). Finally, when the two FEP films gradually come close to each other again, the potential difference between the two electrodes will build, resulting in a reversed current flow in the external circuit (Figure 4c(iv)).

As displayed in Figures 4d and S10, all of the peak outputs (V_{oc} , I_{sc} , and Q_{sc}) increase with the wind speed from 107 V, 2 μA , and 20 nC at 1.55 m s^{-1} to 331 V, 18 μA , and 214 nC at 10.78 m s^{-1} because of the increasing of contact area between the triboelectric layers. The peak output power of 2.7 mW is obtained under a resistance of $100 \text{ M}\Omega$ at 6.96 m s^{-1} (Figure 4e). To further optimize its output performance, the length–width ratio of the FS-TENG is evaluated while the total surface area of the FEP film remains constant. According to the measured results shown in Figure 4f, we found that the V_{oc} , I_{sc} , and Q_{sc} all increase at first with the length–width ratio increase and then decrease. The maximum output performance can be obtained at the length–width ratio of 4:1. The possible explanation is as follows: when the surface area of the FEP film

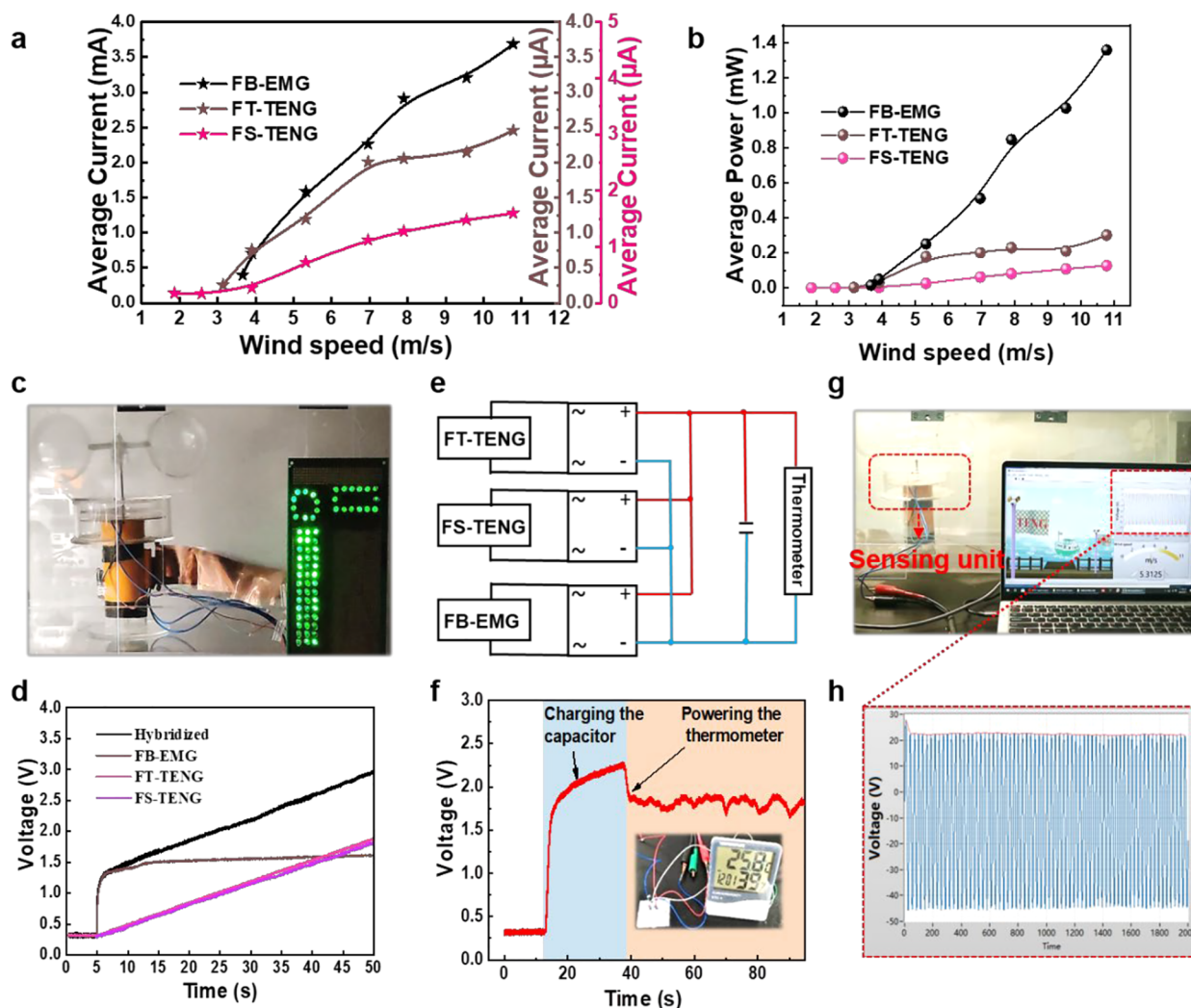


Figure 5. Demonstration of FTEHG for broadband wind energy harvesting and self-powered wind speed sensor. (a) Average output current and (b) power of the FT-TENG, FB-EMG, and FS-TENG at various wind speeds. (c) Photograph of FTEHG for powering LEDs individually and simultaneously. (d) Comparison of FTEHG for charging the capacitor simultaneously and individually. (e) Electric circuit of the FTEHG for building the self-powered systems. (f) Demonstration of FTEHG for powering electronic devices. (g) Photograph of FTEHG for real-time wind speed sensing. (h) Output voltage signal and corresponding frequency.

remains constant, the effective contact area first increases with the film length; once the length reaches a certain value, the FEP film will bend because of the soft characteristics of the ultrathin film, which is harmful for the charge transfer in the contact–separation process of the two films, ultimately resulting in the output performance decreasing with further length increase. Consequently, we choose the 4:1 as the optimal length–width ratio value for practical application, and its detailed output performance and photographs are shown in Figure S11.

Performance Analysis and Application of the FTEHG.

As illustrated in Figure S11, an energy flow diagram for scavenging wind energy is achieved by integration of the TENG and EMG. The average output current and output power of the three parts are measured separately (Figures 5a,b and S12), which indicates that the FB-EMG has the higher average output current and power, but two TENGs have a lower response wind speed, which is consistent with the results mentioned above. Therefore, the hybridization of EMG and TENG is a sensible choice to effectively scavenge mechanical energy in the environment (Note S1). To demonstrate the

capability of the FTEHG as a practical power source, it was directly connected with commercial LEDs without any rectifier or energy storage unit. The photographs of lit LEDs are shown in Figure 5c and Movie S1. As the wind speed increases, the LEDs are gradually lighted sequentially by the FS-TENG, FT-TENG, and FB-EMG, which results from the different response wind speed of the three parts, providing solid evidence of the wide working frequency of the FTEHG. Figure 5d presents the voltage curve of a capacitor with a capacitance of $47 \mu\text{F}$ charged by the FT-TENG, FB-EMG, FS-TENG, and FTEHG at the wind speed of 6.96 m s^{-1} . The charging rate of FTEHG is greater than that of FT-TENG and FS-TENG, and the charging voltage of the FTEHG is much higher than the output voltage of the FB-EMG because of the high output voltage characteristics of the TENG. As displayed in the circuit diagram of the self-powered system, the hybrid nanogenerator and the capacitor are connected by a full-wave rectifier to drive a thermometer (Figure 5e). The thermometer was powered and continuously worked without extra power supply, as shown in Figure 5f and Movie S2.

In addition, the FTEHG can be used to construct a self-powered sensor system. Because the rotation frequency of FT-TENG is proportional to the wind speed, we use the FTEHG as wind speed sensor to realize real-time wind speed monitoring, as shown in [Figure 5g](#) and [Movie S3](#). When the rotator of the FT-TENG begins revolving, the movement frequency of the rotator is obtained by analyzing the peak numbers of the output voltage signal in a computer program ([Figure 5h](#)). The program edited in the computer will automatically calculate the corresponding wind speed according to the entered linear relationship between the frequency and wind speed, which shows great application prospects in real-time and self-powered wind speed monitoring.

In summary, we have demonstrated a multifunctional FTEHG with broadband working range for effective wind energy harvesting and self-powered wind speed sensing. The FTEHG combined the high conversion efficiency of a TENG at low wind speed and high output performance of an EMG at high wind speed. Because a light and soft FEP film is introduced into this structure, the FS-TENG can even work in a light breeze. Therefore, our device not only has high electric output performance but also possesses the feature of wide frequency response, which contribute to its ability to harvest various levels of wind energy to maximize the utilization of renewable wind energy in the environment. The wind speed response range of the FTEHG is from 1.55 to 15 m s⁻¹. The FTEHG successfully charged a 47 μF capacitor to 1.5 V within 4 s under 6.96 m s⁻¹ and continuously powered a thermometer. In addition, according to the linear relationship between the frequency of the FT-TENG and wind speed, FT-TENG has been demonstrated to be a wind speed sensor. This work paves the way for harvesting wider range of wind speed energy by triboelectric–electromagnetic hybrid nanogenerators, which has great potential for wind energy harvesting and sensing in remote areas.

EXPERIMENTAL SECTION

Fabrication of FT-TENG. The FT-TENG was composed of two parts: a stator and a rotator. The stator was made up of a commercial printed circuit board (PCB) with 10 sectors shaped as triboelectric electrodes, whose diameter is 100 mm; the angle of each sector is 35°. The angle between adjacent sectors is 1°. The rotator was fabricated by an acrylic disk, and the FEP film has a thickness of 50 μm. The acrylic disk was cut by a laser cutter and divided into five sectors with the diameter of 100 mm, which has the same sector shape structure as the rotator, and five pieces of FEP film were fixed on it as the triboelectric dielectric layer. A ceramic bearing was installed in the center hole of the acrylic disk. One 5 mm and one 13 mm diameter cylinder were used to connect the rotator and stator. The vertical distance between the stator and rotator is 3 mm. The total weight of the FT-TENG is 36 g.

Fabrication of FB-EMG. The FB-EMG also consisted of two parts: a stator and a rotator. The stator was a cylinder (diameter, 50 mm; height, 5 cm), which was made by 3D printing with PLA material, and four magnets are adhered to the inner wall of the cylinder. The rotator contains four homemade coils, and each coil contains 200 turns. The four coils were connected in series, which was fixed on a cross-shaped acrylic sheet. The total weight of FB-EMG is 175 g, and the total weight of four coils is 24.38 g.

Fabrication of FS-TENG. The contact–separation mode TENG was constructed by two FEP films (thickness: 100 μm),

and magnetron sputtering technology was used to deposit Cu as electrode on the back of the two films. The gap distance between two FEP films is 10 mm. The total weight of the FS-TENG is 3.2 g, and the area of the FEP film is 55 cm².

Assembling the FTEHG. The FT-TENG was placed on the top of the FB-EMG, and the FB-EMG and wind cup has the same rotation axis, which means that the rotator of the FT-TENG and FB-EMG revolve synchronously. In addition, the FS-TENG was fixed on the outer wall of the FB-EMG. The total weight of the FTEHG is 318 g.

Characterization and Measurement. The electric outputs of the hybrid nanogenerator were tested by a programmable electrometer (Keithley Instruments model 6514). The surface morphology was characterized by a field emission scanning electron microscope (Hitachi SU8020).

ASSOCIATED CONTENT

Supporting Information

The Supporting Information is available free of charge at <https://pubs.acs.org/doi/10.1021/acsenerylett.1c00244>.

Optical images of the FT-TENG, FB-EMG, and FS-TENG; potential simulation of FT-TENG; output performance of the FT-TENG with various distances between the rotator and stator; output peak current and power of the FT-TENG; minimum responsive wind speed and corresponding output performance of the FT-TENG at different distances between the rotator and stator; photographs of the FT-TENG; photographs of the FB-EMG; output performance of two FB-EMGs at various wind speeds; photographs of FEP films with different length–width ratios and their corresponding output performance of the FS-TENG; output performance of the FS-TENG at various wind speeds; output current of three nanogenerators at various wind speeds; Tables S1–S3; Note 1 ([PDF](#))

Video S1: Lighting LED process of the FTEHG from low wind speed to high wind speed to verify the broadband characteristics of FTEHG ([MP4](#))

Video S2: FTEHG used to continually power a thermometer ([MP4](#))

Video S3: FTEHG used as wind sensor ([MP4](#))

AUTHOR INFORMATION

Corresponding Author

Zhong Lin Wang – *Beijing Institute of Nanoenergy and Nanosystems, Chinese Academy of Sciences, Beijing 100083, P.R. China; College of Nanoscience and Technology, University of Chinese Academy of Sciences, Beijing 100049, P.R. China; School of Materials Science and Engineering, Georgia Institute of Technology, Atlanta, Georgia 30332, United States; orcid.org/0000-0002-5530-0380; Email: zhong.wang@mse.gatech.edu*

Authors

Cuiying Ye – *Beijing Institute of Nanoenergy and Nanosystems, Chinese Academy of Sciences, Beijing 100083, P.R. China; College of Nanoscience and Technology, University of Chinese Academy of Sciences, Beijing 100049, P.R. China*

Kai Dong – *Beijing Institute of Nanoenergy and Nanosystems, Chinese Academy of Sciences, Beijing 100083, P.R. China;*

College of Nanoscience and Technology, University of Chinese Academy of Sciences, Beijing 100049, P.R. China

Jie An – Beijing Institute of Nanoenergy and Nanosystems, Chinese Academy of Sciences, Beijing 100083, P.R. China; College of Nanoscience and Technology, University of Chinese Academy of Sciences, Beijing 100049, P.R. China

Jia Yi – Beijing Institute of Nanoenergy and Nanosystems, Chinese Academy of Sciences, Beijing 100083, P.R. China; College of Nanoscience and Technology, University of Chinese Academy of Sciences, Beijing 100049, P.R. China

Xiao Peng – Beijing Institute of Nanoenergy and Nanosystems, Chinese Academy of Sciences, Beijing 100083, P.R. China; College of Nanoscience and Technology, University of Chinese Academy of Sciences, Beijing 100049, P.R. China

Chuan Ning – Beijing Institute of Nanoenergy and Nanosystems, Chinese Academy of Sciences, Beijing 100083, P.R. China; College of Nanoscience and Technology, University of Chinese Academy of Sciences, Beijing 100049, P.R. China

Complete contact information is available at:

<https://pubs.acs.org/10.1021/acsenerylett.1c00244>

Author Contributions

^δC.Y., K.D., and J.A. contributed equally to this work.

Notes

The authors declare no competing financial interest.

ACKNOWLEDGMENTS

The authors are grateful for the support received from the National Key R&D Project from Minister of Science and Technology (Grant No. 2016YFA0202704), the Beijing Municipal Natural Science Foundation (Grant No. 2212052), the Shanghai Sailing Program (Grant No. 19S28101), and the Fundamental Research Funds for the Central Universities (Grant No. 19D128102).

REFERENCES

- (1) Wang, Z. L. Entropy theory of distributed energy for internet of things. *Nano Energy* **2019**, *58*, 669–672.
- (2) Chen, B.; Yang, Y.; Wang, Z. L. Scavenging Wind Energy by Triboelectric Nanogenerators. *Adv. Energy Mater.* **2018**, *8* (10), 1702649.
- (3) Yang, Y.; Zhu, G.; Zhang, H.; Chen, J.; Zhong, X.; Lin, Z.; Su, Y.; Bai, P.; Wen, X.; Wang, Z. L. Triboelectric Nanogenerators as New Energy Technology for Self-Powered Systems and as Active Mechanical Sensors. *ACS Nano* **2013**, *7* (10), 9461–9468.
- (4) Wang, Z. L. Triboelectric Nanogenerator (TENG)-Sparking an Energy and Sensor Revolution. *Adv. Energy Mater.* **2020**, *10* (17), 2000137.
- (5) Dong, K.; Peng, X.; An, J.; Wang, A.; Luo, J.; Sun, B.; Wang, J.; Wang, Z. L. Shape adaptable and highly resilient 3D braided triboelectric nanogenerators as e-textiles for power and sensing. *Nat. Commun.* **2020**, *11* (1), 2868.
- (6) Peng, X.; Dong, K.; Ye, C.; Jiang, Y.; Zhai, S.; Cheng, R.; Liu, D.; Gao, X.; Wang, J.; Wang, Z. L. A breathable, biodegradable, antibacterial, and self-powered electronic skin based on all-nanofiber triboelectric nanogenerators. *Sci. Adv.* **2020**, *6* (26), eaba9624.
- (7) Ning, C.; Dong, K.; Cheng, R.; Yi, J.; Ye, C.; Peng, X.; Sheng, F.; Jiang, Y.; Wang, Z. L. Flexible and Stretchable Fiber-Shaped Triboelectric Nanogenerators for Biomechanical Monitoring and Human-Interactive Sensing. *Adv. Funct. Mater.* **2021**, *31* (4), 2006679.
- (8) Li, S.; Liu, D.; Zhao, Z.; Zhou, L.; Yin, X.; Li, X.; Gao, Y.; Zhang, C.; Zhang, Q.; Wang, J.; Wang, Z. L. A Fully Self-Powered Vibration

Monitoring System Driven by Dual-Mode Triboelectric Nanogenerators. *ACS Nano* **2020**, *14* (2), 2475–2482.

(9) Liang, X.; Jiang, T.; Feng, Y.; Lu, P. J.; An, J.; Wang, Z. L. Triboelectric Nanogenerator Network Integrated with Charge Excitation Circuit for Effective Water Wave Energy Harvesting. *Adv. Energy Mater.* **2020**, *10* (40), 2002123.

(10) Ren, Z.; Wang, Z.; Liu, Z.; Wang, L.; Guo, H.; Li, L.; Li, S.; Chen, X.; Tang, W.; Wang, Z. L. Energy Harvesting from Breeze Wind (0.7–6 m s⁻¹) Using Ultra-Stretchable Triboelectric Nanogenerator. *Adv. Energy Mater.* **2020**, *10* (36), 2001770.

(11) Bae, J.; Lee, J.; Kim, S.; Ha, J.; Lee, B. S.; Park, Y.; Choong, C.; Kim, J. B.; Wang, Z. L.; Kim, H. Y.; et al. U. I. Flutter-driven triboelectrification for harvesting wind energy. *Nat. Commun.* **2014**, *5*, 4929.

(12) Xi, Y.; Guo, H.; Zi, Y.; Li, X.; Wang, J.; Deng, J.; Li, S.; Hu, C.; Cao, X.; Wang, Z. L. Multifunctional TENG for Blue Energy Scavenging and Self-Powered Wind-Speed Sensor. *Adv. Energy Mater.* **2017**, *7* (12), 1602397.

(13) Zeng, Q.; Wu, Y.; Tang, Q.; Liu, W.; Wu, J.; Zhang, Y.; Yin, G.; Yang, H.; Yuan, S.; Tan, D.; Hu, C.; Wang, X. A high-efficient breeze energy harvester utilizing a full-packaged triboelectric nanogenerator based on flow-induced vibration. *Nano Energy* **2020**, *70*, 104524.

(14) Yang, Y.; Zhu, G.; Zhang, H.; Chen, J.; Zhong, X.; Lin, Z.; Su, Y.; Bai, P.; Wen, X.; Wang, Z. L. Triboelectric Nanogenerator for Harvesting Wind Energy and as Self-Powered Wind Vector Sensor System. *ACS Nano* **2013**, *7* (10), 9461–9468.

(15) Wang, J.; Ding, W.; Pan, L.; Wu, C.; Yu, H.; Yang, L.; Liao, R.; Wang, Z. L. Self-Powered Wind Sensor System for Detecting Wind Speed and Direction Based on a Triboelectric Nanogenerator. *ACS Nano* **2018**, *12* (4), 3954–3963.

(16) Sun, W.; Ding, Z.; Qin, Z.; Chu, F.; Han, Q. Wind energy harvesting based on fluttering double-flag type triboelectric nanogenerators. *Nano Energy* **2020**, *70*, 104526.

(17) Wang, Q.; Zou, H.; Zhao, L.; Li, M.; Wei, K.; Huang, L.; Zhang, W.-M. A synergetic hybrid mechanism of piezoelectric and triboelectric for galloping wind energy harvesting. *Appl. Phys. Lett.* **2020**, *117* (4), 043902.

(18) Zhao, L.; Zou, H.; Gao, Q.; Yan, G.; Wu, Z.; Liu, F.; Wei, K.; Yang, B.; Zhang, W. Design, modeling and experimental investigation of a magnetically modulated rotational energy harvester for low frequency and irregular vibration. *Sci. China: Technol. Sci.* **2020**, *63* (10), 2051–2062.

(19) Zhao, L.; Zou, H.; Yan, G.; Liu, F.; Tan, T.; Wei, K.; Zhang, W. Magnetic coupling and flextensional amplification mechanisms for high-robustness ambient wind energy harvesting. *Energy Convers. Manage.* **2019**, *201*, 112166.

(20) Zhao, L.; Zou, H.; Yan, G.; Liu, F.; Tan, T.; Zhang, W.; Peng, Z.; Meng, G. A water-proof magnetically coupled piezoelectric-electromagnetic hybrid wind energy harvester. *Appl. Energy* **2019**, *239*, 735–746.

(21) Zou, H.; Zhao, L.; Gao, Q.; Zuo, L.; Liu, F.; Tan, T.; Wei, K.; Zhang, W. Mechanical modulations for enhancing energy harvesting: Principles, methods and applications. *Appl. Energy* **2019**, *255*, 113871.

(22) Zou, H.; Li, M.; Zhao, L.; Gao, Q.; Wei, K.; Zuo, L.; Qian, F.; Zhang, W. A magnetically coupled bistable piezoelectric harvester for underwater energy harvesting. *Energy* **2021**, *217*, 119429.

(23) Hu, G.; Wang, J.; Su, Z.; Li, G.; Peng, H.; Kwok, K. C. S. Performance evaluation of twin piezoelectric wind energy harvesters under mutual interference. *Appl. Phys. Lett.* **2019**, *115* (7), 073901.

(24) Sezer, N.; Koç, M. A comprehensive review on the state-of-the-art of piezoelectric energy harvesting. *Nano Energy* **2021**, *80*, 105567.

(25) Shao, H.; Wen, Z.; Cheng, P.; Sun, N.; Shen, Q.; Zhou, C.; Peng, M.; Yang, Y.; Xie, X.; Sun, X. Multifunctional power unit by hybridizing contact-separate triboelectric nanogenerator, electromagnetic generator and solar cell for harvesting blue energy. *Nano Energy* **2017**, *39*, 608–615.

(26) Guo, H.; Wen, Z.; Zi, Y.; Yeh, M.-H.; Wang, J.; Zhu, L.; Hu, C.; Wang, Z. L. A Water-Proof Triboelectric-Electromagnetic Hybrid

Generator for Energy Harvesting in Harsh Environments. *Adv. Energy Mater.* **2016**, *6* (6), 1501593.

(27) Zhang, B.; Chen, J.; Jin, L.; Deng, W.; Zhang, L.; Zhang, H.; Zhu, M.; Yang, W.; Wang, Z. L. Rotating-Disk-Based Hybridized Electromagnetic-Triboelectric Nanogenerator for Sustainably Powering Wireless Traffic Volume Sensors. *ACS Nano* **2016**, *10* (6), 6241–6247.

(28) Zhang, Y.; Cao, J.; Zhu, H.; Lei, Y. Design, modeling and experimental verification of circular Halbach electromagnetic energy harvesting from bearing motion. *Energy Convers. Manage.* **2019**, *180*, 811–821.

(29) Chen, Y.; Cheng, Y.; Jie, Y.; Cao, X.; Wang, N.; Wang, Z. L. Energy harvesting and wireless power transmission by a hybridized electromagnetic-triboelectric nanogenerator. *Energy Environ. Sci.* **2019**, *12* (9), 2678–2684.

(30) Wen, Z.; Guo, H.; Zi, Y.; Yeh, M. H.; Wang, X.; Deng, J.; Wang, J.; Li, S.; Hu, C.; Zhu, L.; Wang, Z. L. Harvesting Broad Frequency Band Blue Energy by a Triboelectric-Electromagnetic Hybrid Nanogenerator. *ACS Nano* **2016**, *10* (7), 6526–6534.

(31) Wang, X.; Wen, Z.; Guo, H.; Wu, C.; He, X.; Lin, L.; Cao, X.; Wang, Z. L. Fully Packaged Blue Energy Harvester by Hybridizing a Rolling Triboelectric Nanogenerator and an Electromagnetic Generator. *ACS Nano* **2016**, *10* (12), 11369–11376.

(32) Zhang, C.; Tang, W.; Han, C.; Fan, F.; Wang, Z. L. Theoretical comparison, equivalent transformation, and conjunction operations of electromagnetic induction generator and triboelectric nanogenerator for harvesting mechanical energy. *Adv. Mater.* **2014**, *26* (22), 3580–91.

(33) Zi, Y.; Guo, H.; Wen, Z.; Yeh, M. H.; Hu, C.; Wang, Z. L. Harvesting Low-Frequency (<5 Hz) Irregular Mechanical Energy: A Possible Killer Application of Triboelectric Nanogenerator. *ACS Nano* **2016**, *10* (4), 4797–805.

(34) Wang, P.; Pan, L.; Wang, J.; Xu, M.; Dai, G.; Zou, H.; Dong, K.; Wang, Z. L. An Ultra-Low-Friction Triboelectric-Electromagnetic Hybrid Nanogenerator for Rotation Energy Harvesting and Self-Powered Wind Speed Sensor. *ACS Nano* **2018**, *12* (9), 9433–9440.

(35) Zhang, Y.; Zeng, Q.; Wu, Y.; Wu, J.; Yuan, S.; Tan, D.; Hu, C.; Wang, X. An Ultra-Durable Windmill-Like Hybrid Nanogenerator for Steady and Efficient Harvesting of Low-Speed Wind Energy. *Nano-Micro Lett.* **2020**, *12* (1), 175.

(36) Fan, X.; He, J.; Mu, J.; Qian, J.; Zhang, N.; Yang, C.; Hou, X.; Geng, W.; Wang, X.; Chou, X. Triboelectric-electromagnetic hybrid nanogenerator driven by wind for self-powered wireless transmission in Internet of Things and self-powered wind speed sensor. *Nano Energy* **2020**, *68*, 104319.

(37) Francis Beaufort. Beaufort Scale. <https://wenku.baidu.com/view/ce24ff5c83c4bb4cf7ecd1fc.html> (accessed 2020-10).

(38) Beijing Youth Daily. Beijing is getting warmer by 0.45°C per decade. http://bj.cma.gov.cn/xwzx/mtjj/201903/t20190311_614178.html (accessed 2020-10).